PUBLICATION REQUEST

ORIGINATOR: Michele Rienecker, Code 971

TITLE: Mechanism for surface warming in the Equatorial Pacific Ocean during 1994-95

AUTHORS: Anna Borovikov, Michele M. Rienecker, and Paul S. Schopf

Significant findings:

This paper explores the capability of the Poseidon ocean model, used by NSIPP, of reproducing the interannual SST variations observed by AVHRR and the TAO moorings during 1994-95. Since the model shows skill for the large anomalies during this period, the dynamical and thermodynamical mechanisms responsible for the anomalies are investigated. Since the dominant mechanisms are consistent between simulations forced by two different wind products (one satellite-derived, one in situ-based), the mechanisms inferred from the model seem to be robust. Unlike the 1982-83 and 1997-98 El Ninos, when the maximum SST anomaly was found in the eastern basin, the maximum anomaly during 1994-95 was in the central basin. Also, whereas the dominant mechanism for the SST anomaly during 1982-83 had been found to be advection across the entire basin, during 1994-95, external heat flux anomalies were important in the western basin, and advection and vertical mixing in the eastern basin.

PUBLICATION REQUEST:

TITLE: Mechanism for surface warming in the Equatorial Pacific Ocean during 1994-95

AUTHORS: Anna Borovikov, Michele M. Rienecker, and Paul S. Schopf

ORIGINATOR: Michele Rienecker, Code 971

Program relevance: Seasonal to Interannual Variability

Mechanisms for Surface Warming in the Equatorial Pacific Ocean During 1994-95

Anna Borovikov
SAIC, General Sciences Corporation, Beltsville, Maryland

Michele M. Rienecker
NASA Seasonal-to-Interannual Prediction Project, Oceans and Ice Branch, Laboratory for Hydrospheric Processes, NASA/Goddard Space Flight Center, Greenbelt, Maryland

Paul S. Schopf
Institute for Computational Sciences and Informatics, George Mason University, Fairfax, Virginia

1 December 1999

To be submitted to J. Climate

Abstract

Mechanisms controlling the variation in sea surface temperature (SST) during the 1994-1995 warm event in the equatorial Pacific were investigated through ocean model simulations. In addition, the mechanisms of the climatological SST cycle were investigated. The dominant mechanisms governing the seasonal cycle of SST vary significantly across the basin. In the western Pacific the annual cycle of SST is primarily in response to external heat flux. In the central basin the magnitude of zonal advection is comparable to that of the external heat flux. In the eastern basin the role of zonal advection is reduced and the vertical mixing is more important. In the easternmost equatorial Pacific the vertical entrainment contribution is as large as that of vertical diffusion. The model estimate of the vertical mixing contribution to the mixed layer heat budget compared well with estimates obtained by analysis of observations using the same diagnostic vertical mixing scheme. During 1994-1995 the largest positive SST anomaly was observed in the mid-basin and was related to reduced latent heat flux due to weak surface winds. In the western basin the initial warming was related to enhanced external heating and reduced cooling effects of both vertical mixing and horizontal advection associated with weaker than usual wind stress. In the eastern Pacific where winds were not significantly anomalous throughout 1994-1995, only a moderate warm surface anomaly was detected. This is in contrast to strong El Niño events where the SST anomaly is largest in the eastern basin and, as shown by previous studies, the anomaly is due to zonal advection rather than anomalous surface heat flux. The end of the warm event was marked by cooling in July 1995 everywhere across the equatorial Pacific.

1. INTRODUCTION

The first half of the 1990's was marked by a series of warm events of various amplitudes and duration in the equatorial Pacific Ocean. The focus of this study, the 1994-1995 warming is the earliest of the best observed events, since by this time the implementation of the Tropical Atmosphere-Ocean (TAO) Array, under the Tropical Ocean-Global Atmosphere (TOGA) Program, was completed, with 65 ATLAS moorings and 5 current meter moorings deployed across the equatorial Pacific.

The relative importance of various processes influencing the annual cycle of the sea surface temperature was investigated by *Kessler et al.* [1998] (hereinafter referred to as KRC) in the eastern equatorial Pacific. Their integration using the Gent-Cane model shows a complicated balance in the cold tongue region, where all terms of the temperature equation are important in the annual cycle of SST. The largest terms in the annual cycle are the external heat flux term and vertical advection. Although zonal advection contributes to a warming tendency throughout the year and meridional advection tends to cool the surface during boreal spring, overall the 3D advective effect is small. *Chen et al.* [1994] (hereinafter referred to as CBR), also using the Gent-Cane model, analyzed the annual cycle of the mixed layer heat budget across the entire equatorial Pacific. Their model analysis of the temperature equation showed increasing magnitude in the external heat flux from west to east. The next important term in the heat balance of the upper layer, after the external heat flux, was found to be the vertical advection. Zonal advection was more important in the central basin than in either the west or the east. In the eastern Pacific CBR show that the vertical diffusion plays a significant role, although not as large as the vertical advection. Neither KRC nor CBR found the vertical diffusion contribution to be as large as *Hayes et al.* [1991] estimated from observations.

Other studies have investigated the balances in the mixed layer during different El Niño events. *Harrison et al.* [1990] found that during the 1982-1983 El Niño the warming in the central basin was related to the anomalous eastward surface advection of warm water and

that external heat flux did not contribute to anomalous temperatures. Further to the east although zonal advection was still significant in their model, other terms, like meridional advection, contributed to the warming. The successive cooling back to climatological temperatures was initiated by increased vertical advection of cold water and once the cooling began the contribution of horizontal advection was found to be significant. An observational study of El Niño conditions was conducted by *Hayes et al.* [1991]. Their analysis of the 1986-1987 El Niño also suggests that in the eastern equatorial basin around 110°W no single process dominated the upper layer heat budget. The dominant processes were found to be the external heat flux and the vertical turbulent diffusion of heat out of the bottom of the mixed layer. Zonal advection, while contributing significantly to the mixed layer heat budget, was not strongly correlated with the local SST tendency.

Here, the ocean circulation model by *Schopf et al.* [1995] was used to study the thermodynamical causes of SST variations for the 1994-1995 event in the equatorial Pacific. The ocean model was forced with two different monthly mean surface wind stress analyses. Although, as to be expected, the surface temperature was very sensitive to the surface wind stress, there was a general agreement between the two experiments on most prominent features of the model behavior. Less agreement, however, was found between the model results and observations. *Harrison et al.* [1990], who conducted a similar study of the 1982-1983 El Niño - Southern Oscillation (ENSO) event with a different model, attributed this in part to the imperfect knowledge of the wind stresses. Nevertheless, in spite of their model's short-comings, it successfully simulated large anomalies in SST. The same is found in this study.

The paper is organized as follows. In section 2 the observational data and its role in experiment design and the ocean model used to compute the hindcasts of the analyzed period are presented. The model performance is evaluated by direct comparison of the model and observed fields as well as by matching the sign of the sea surface temperature time derivative. Section 3 gives an overview of the climatological mixed layer heat budget and in section 4

the effects of the various terms contributing to the surface temperature changes during the analysis period are considered in detail. The last section contains discussion and summary.

2. Model and Data

2.1. Observational Data

The TAO Array, consisting of nearly 70 moored buoys spanning the equatorial Pacific as shown in figure 1 measures oceanographic and surface meteorological variables: air temperature, relative humidity, surface winds, sea surface temperatures and subsurface temperatures down to a depth of 500 meters [*McPhaden et al.* 1998]. The availability of the SST time series from the moorings spanning the equator is shown in figure 2. By 1994 daily SST measurements became available at approximately uniformly spaced locations across the equatorial Pacific Ocean. For this study the SST time series were formed by averaging data collected at the 3 moorings spanning the equator (2°S, 2°N and equator) at 9 different longitudes: 156°E, 165°E, 180°W, 170°W, 155°W, 140°W, 125°W, 110°W and 95°W, where the most complete records were available.

The evolution of the sea surface temperature as derived from the TOGA TAO observations is shown in the figure 3, obtained through the TAO Web Page (http://www.pmel.noaa.gov/toga-tao/home.html). In late 1994 and early 1995 a warm anomaly was present in the central and eastern basin. The maximum anomaly of 2°C was located just east of the dateline. Anomalies of over 1°C extended to the eastern boundary. In comparison, the maximum warm anomaly of 1.5°C in 1993 was at the date line; during 1991-1992 the maximum anomaly of 2.5°C was located between 160°W and 150°W. In both of these cases anomalies as high as 1.5°C extended to the eastern boundary. For the major El Niño of 1997-1998 the largest anomaly was at the eastern boundary, and reached almost 5°C. In 1995-1996, following the anomalous warming of the central and eastern Pacific, cold anomalies developed with temperatures being 1°C lower than normal.

Another dataset with good spatial coverage and fine time resolution is the Version 4 AVHRR Pathfinder SST, which has been de-clouded using the standard Pathfinder cloud-masking algorithm plus an additional "erosion" filter. It has been processed by *Casey and Cornillon* [1999]. To overcome data gaps due to clouds the data for this study were averaged within boxes extending 4 degrees in latitudes and 5 degrees in longitude centered at the mooring longitudes listed above. Except for a single two week period of persistent cloudiness a time series was obtained comparable in time and space resolution to the TAO data.

The monthly-averaged SST fields based on the satellite observations from 10°S to 10 °N are shown in figure 4. Within this region it can be seen that the interannual change of SST is much smaller off the equator than close to the equator. Superimposed on the annual cycle there are significant differences between 1994 and 1995. Near the equator the interannual changes are manifest in the variability in the shape and extent of the cold tongue. During September - December 1994 the central basin was warmer than during the corresponding months in 1995. Temperatures exceeding 30°C were observed at 170°E-160°W and near the western boundary the surface was at least 1°C colder than during the following year. During the same months in 1995 the highest temperatures were near the western boundary, and the temperature had dropped by 2-4°C at the location of the the warmest anomaly during 1994. During boreal winter 1994-1995 the meridional gradient at and south of the equator in the eastern basin was reduced. In 1995-1996 it was enhanced and the cold tongue extended farther westward than during winter 1993-1994.

2.2. Model and Forcing

The Poseidon reduced-gravity quasi-isopycnal ocean model introduced by *Schopf and Loughe* [1995] was used to study the heat balance of the surface layer. For this study the domain was restricted to the Pacific Ocean with realistic land boundaries. At the southern boundary the model temperature and salinity were relaxed to the Levitus (1994) climatology. The horizontal resolution of the model was 1° in longitude; and in the meridional direction a

stretched grid was used, varying from 1/3° at the equator to 1° at 10°S and 10°N and beyond. The generalized vertical coordinate of the model includes a turbulent well-mixed surface layer with entrainment parameterized according to a *Kraus-Turner*[1967] bulk mixed layer model. The model described by *Schopf and Loughe* [1995] has been updated to include the effects of salinity [*Yang et al.* 1999]. Surface salinity values are relaxed to the Levitus (1994) climatology with a 15 day timescale. The calculation of the effects of vertical diffusion, implemented once a day, were parameterized through a Richardson number-dependent implicit vertical mixing following the *Pacanowski-Philander* [1981] scheme. The diffusion coefficients were enhanced to simulate convective overturning in cases of gravitationally unstable density profiles. Horizontal diffusion was also computed daily using an 8th order *Shapiro* [1970] filter. The external heat flux was estimated using the atmospheric mixed layer model by *Seager et al.* [1994] with the time-varying air temperature and specific humidity from the NCEP-NCAR reanalysis [*Kalnay et al.*, 1996] and climatological shortwave radiation from the Earth Radiation Budget Experiment (ERBE) [*Harrison et al.*, 1993] and climatological cloudiness from the International Satellite Cloud Climatology Progect (ISCCP) [*Rossow and Schiffer*, 1991].

To test the robustness of the inferred balances, the model was driven with two different wind products: the Special Sensor Microwave Imager (SSM/I) wind analysis based on satellite measurements and the FSU pseudostress analysis from *in situ* observations. The surface wind analysis produced by *Atlas at al.* [1991] is based on the combination of the Defense Meteorological Satellite Program (DMSP) SSM/I data with other conventional data and with the ECMWF 10m surface wind analysis. The surface stress was produced from this analysis using the drag coefficient of *Large and Pond* [1982]. The model output with this forcing is referred to as P-SSMI. The second experiment was conducted with the pseudostress analysis derived from ships and buoys produced at FSU [*Legler and O'Brien*, 1988]. The surface stress was produced from this pseudostress using a constant drag coefficient of 1.3×10^{-3} and that simulation is termed P-FSU. In both cases monthly-averaged forcing was used.

In monthly-averaged climatologies (based on 1988-1997 time series) of zonal and meridional wind stress along the equator (figure 7, lower panels) the SSMI stress tends to be weaker in the central basin with a stronger semiannual signal in τ_x than FSU. In the western basin the FSU stress is westerly year round; near the eastern boundary SSMI has stronger westerly winds than does FSU. The anomalies in zonal stress (figure 7, upper panels) are generally consistent in sign, but the FSU anomalies are stronger than those from SSMI. During 1994-1995, the westerly anomaly was of greater duration and extent in FSU.

The monthly averages of SST fields from the two experiments are shown in figures 5 and 6. The qualitative behavior of the model SST compares well with observations although the amplitude of the temperature variability is lower in the model, especially in P-FSU. The model SST tends to be too low north of the cold tongue in both simulations. Otherwise, the SST structure in P-SSMI agrees better with observations than does P-FSU, which is too cold throughout the tropical Pacific. The meridional variations of SST in the eastern Pacific are also better in P-SSMI throughout most of the 2-year period although the anomaly and gradients during boreal fall and winter 1995 are weak.

To evaluate model performance for the investigation of the SST tendency, $\partial \mathrm{SST}/\partial t$, a comparison was made of the sign of the tendency, pairwise between each model run and each dataset. All the fields were smoothed in time and space by averaging as described above. As might be expected, the two datasets agree reasonably well with periods of disagreement rarely exceeding 2 consecutive months. In the model-data comparisons, less agreement was found, particularly between P-FSU and both datasets at 165°E and between P-FSU and TAO at 110°W. Overall, the SSMI simulation tends to agree better with observations than the FSU simulation. However, one would expect discrepancies in sign for small amplitude changes. The comparison that considers the values of $\partial \mathrm{SST}/\partial t$ with amplitude larger than 0.5°C/month is shown in figure 8 and the months during which the sea surface temperature has changed by less than 0.5°C are left blank. With this discriminating filter very few periods of disagreement remain. Thus the large scale variations in SST are captured well by Poseidon

in this model configuration and from this perspective it is quite suitable for a study of SST variations.

The analysis of the mixed layer heat flux and the evolution of the sea surface temperature that follows are determined from 3-day averaged history files to capture the influence of short time scale variations on the monthly averages.

2.3. Zonal Correlation Scales of $\partial SST/\partial t$

Since the model simulated the equatorial SST variability reliably, it can be used to investigate the mechanisms responsible for these variations across the basin. Spatial averaging is needed for the analysis of large scale processes in the surface heat budget at seasonal and interannual time scales. To guide the selection of regions for averaging, zonal decorrelation scales of $\partial \mathrm{SST}/\partial t$ were estimated from the model runs. The zonal decorrelation scales are relatively large (15°-20°) in the western basin and shorter (5°-10°) in the eastern Pacific. Using these estimates six regions for detailed study of surface layer heat budget were selected. Each of these regions extends meridionally from 2°S to 2°N and their zonal extent is as follows, from west to east: western region (denoted WW) is 155°E-175°E, western central region (WC) is 175°E-165°W, central western region (CW) is 165°W-145°W, central eastern region (CE) is 145°W-110°W, eastern central region (EC) is 110°W-95°W and eastern region (EE) is 95°W-85°W.

3. Surface Layer Climatology

To highlight the general properties of the mixed layer heat budget and to establish the reference for the analysis of the evolution of $h\partial T/\partial t$ during the warming event of 1994-1995 the climatological mixed layer heat budget is discussed first. To evaluate the realism of Poseidon's performance in the equatorial Pacific, the mixed layer heat budget climatology based on Poseidon output is compared with the typical annual cycle of the mixed layer

heat budget in the eastern equatorial Pacific as estimated by KRC and a climatological annual cycle from the CBR study of the tropical Pacific sea surface temperature. In both works essentially the same Gent-Cane model was used. The heat budget climatology is also compared with the work by *Hayes et al.* [1991], whose estimates of SST variability and the processes governing it were based on observations alone.

The surface mixed layer evolves according to the heat content equation:

$$\frac{\partial hT}{\partial t} + \nabla \cdot (\mathbf{v}hT) + \frac{\partial w_e T}{\partial \zeta} = \frac{\partial}{\partial \zeta}\left(\frac{\kappa}{h}\frac{\partial T}{\partial \zeta}\right) + \frac{\partial Q}{\partial \zeta} + h\mathcal{F}_H(T), \tag{1}$$

and the continuity equation:

$$\frac{\partial h}{\partial t} + \nabla \cdot (\mathbf{v}h) + \frac{\partial w_e}{\partial \zeta} = 0. \tag{2}$$

Here T is the potential temperature, h is the mixed layer thickness, $\mathbf{v}$ is the horizontal velocity, ζ is the generalized vertical coordinate, κ is the vertical diffusivity coefficient, Q is the external heat flux (latent, sensible and radiative fluxes at the surface with penetrative short-wave radiation). The entrainment velocity at the base of the mixed layer, w_e, is determined according to a Kraus-Turner bulk mixed layer model (see *Schopf and Loughe* [1995] for details). $\mathcal{F}_H(T)$ is a Shapiro filter horizontal smoothing operator. As mentioned above, the model now includes a prognostic salinity equation and salinity variations impact the heat budget of the mixed layer through the entrainment velocity, w_e, which depends on the surface buoyancy flux and density gradient at the base of the mixed layer.

3.1. Mixed Layer Depth

From the analysis of the continuity equation, it can be seen that the nature of the annual cycle of mixed layer depth (MLD) varies from west to east (see figure 9 and 10). In the western basin (WW region) the MLD shows a strong annual signal being the deepest (about 45 m) in boreal winter and the shallowest (about 30 m) during the late summer/early autumn. Analysis of the terms in the continuity equation shows that the meridional divergence, which has the largest magnitude, is balanced by vertical entrainment and zonal convergence. In the

WC region the ML is generally deeper, varying between 40 and 60 m. Rapid deepening takes place in late boreal autumn/early winter and shoaling in early spring. From May through October the monthly-mean MLD remains fairly constant. A weak semiannual component is noticeable in MLD variation, especially in P-SSMI. The dominant terms in the continuity equation are meridional divergence due to strong zonal winds and vertical entrainment. The magnitude of these terms increases from west to east. Zonal convergence remains small. The strongest meridional divergence and vertical entrainment appear in mid-basin (CW and CE regions). In the CW region the MLD signal has strong semiannual component with maximum in January (60-65 m) only slightly larger that the maximum in July (53-58 m). The ML shoals in April and October to 40-45 m. In the CE region the relation between terms in the continuity equation is similar to that in the CW region, but the semiannual component of the MLD weakens. Toward the east, the semiannual signal is further diminished. In the EC region, the spring minimum in ML depth is about 15-17 m and from July through December the ML is nearly level at 25-27 m. While the relative role of the terms in the continuity equation is the same, meridional divergence and vertical entrainment have smaller magnitude than in the mid-basin. In the easternmost region (EE) zonal divergence becomes equally important in the ML dynamics due to strong meridional wind stress in this area. The MLD varies from about 15 m in March-April to about 30 m in July-November. The variations are consistent between P-FSU and P-SSMI.

3.2. Surface Heat Budget

To separate the mass conservation balance from the energy conservation balance it is necessary to subtract (2) multiplied by the temperature T from (1):

$$h\frac{\partial T}{\partial t} + h\mathbf{v}\cdot\nabla T + w_e\frac{\partial T}{\partial \zeta} = \frac{\partial}{\partial \zeta}\left(\frac{\kappa}{h}\frac{\partial T}{\partial \zeta}\right) + \frac{\partial Q}{\partial \zeta} + h\mathcal{F}_H(T). \tag{3}$$

The contributions of the various thermodynamic processes in the SST variations to the heat budget for the surface mixed layer were evaluated. It was found that the contribution of the filtering term to the budget analyzed below is small when compared with all other

terms in the equation, so it is neglected. In the following sections the influence of the zonal and meridional advection, vertical advection, vertical mixing (diffusion) and external heat flux on the sea surface temperature tendency is analyzed.

Rearrangement of equation (3), neglecting the horizontal filtering term, gives:

$$h\frac{\partial T}{\partial t} = -hu\frac{\partial T}{\partial x} - hv\frac{\partial T}{\partial y} - w_e\frac{\partial T}{\partial \zeta} + \frac{\partial}{\partial \zeta}\left(\frac{\kappa}{h}\frac{\partial T}{\partial \zeta}\right) + \frac{\partial Q}{\partial \zeta}. \tag{4}$$

For convenience the heat flux due to each of the terms in the above equation are denoted as follows:

$$\rho_0 C_p h\frac{\partial T}{\partial t} = Q_{zon.adv.} + Q_{mer.adv.} + Q_{vert.adv.} + Q_{vert.mix.} + Q_{ext.heat}.$$

Each term of this equation was evaluated at every model grid point from the 3-day averaged history file. Monthly means and spatial averages were then computed over the analysis regions described above in section 2..

For the climatology displayed in figure 11, data from 1988 through 1997 was used which was available for both P-FSU and P-SSMI. Note the change in scales for different analysis regions. The sum of all the terms on the right hand side of equation (4) is almost indistinguishable from the time series of $\rho_0 C_p h\partial T/\partial t$ computed directly from the model temperature fields so the heat budget was closed adequately with 3-day averages.

The climatologies based on P-FSU and P-SSMI model runs are not discussed separately since in general they exhibit similar qualitative behavior. However significant observed differences are acknowledged and possible causes are analyzed.

The relative role of different terms in the heat budget varies greatly in the zonal direction. As can be seen in figure 11 in the WW region, 155°E-175°E, the external heat flux term is of moderate amplitude with maximum values of about 40 Wm^{-2} and is highly correlated with $h\partial T/\partial t$ which has a distinct semiannual variation. The warming tendency of the external heat flux is almost balanced by the cooling tendency of zonal advection, vertical advection and vertical mixing, all comparable in magnitude, about 10 Wm^{-2}. The meridional advection term changes sign, but its amplitude is small and it has little influence on the overall balance.

Zonal advection is strongest during boreal winter when it is responsible for the cooling tendency of SST. Primarily because of the deeper mixed layer at this time (see figure 9) in response to stronger meridional stress, since the westward zonal current peaks in March. The zonal advection term is negligible during summer when the zonal current is weak.

In the WC region, 175°E-165°W, the amplitude of the external heat flux is larger, up to 70 Wm^{-2}, and so is the amplitude of the zonal advection. The balance remains much the same as for WW. Zonal advection has a cooling tendency in the WC region, except during late boreal spring when the flow is weak and the mixed layer is thin. The vertical advection contribution is slightly larger in the WC region than in the WW region.

In the CW region, 165°W-145°W, the effect of zonal advection, reaching values of -50 Wm^{-2} is larger than elsewhere along the equator due to large temperature gradients. In late boreal spring/early summer it clearly contributes to a warming tendency, counterbalancing the effects of diapycnal fluxes from vertical advection and diffusion and very weak cooling due to meridional advection. In both the WC and CW regions the annual cycle of wind patterns is such that easterly winds usually diminish during boreal spring and, in response, the westward current weakens or even reverses direction. Both current and mixed layer depth have a strong semi-annual signal. Vertical and meridional advection and vertical mixing do not vary much in the CW region. Their contributing roles, although much smaller than zonal advection, are clearly important in balancing the surface heating.

In the CE region, 145°W-110°W, the picture is quite different: the seasonal cycle of SST is dominated by the annual signal and here vertical mixing plays the dominant role in balancing the external heat flux. However, both vertical and meridional advection are more important in the balance than farther west and contribute to surface cooling year long, consistent with KRC. Cooling by vertical advection usually exceeds (by about 20 Wm^{-2}) the warming tendency of zonal advection which is more variable. In the P-FSU climatology the zonal advection term does not vary much and is always positive in the CE region, while in P-SSMI its variations are more noticeable and it becomes negative in July-August and in

December-January. This is the region where the zonal velocity and mixed layer depth have stronger semi-annual signals in P-SSMI than in P-FSU. The zonal advection contribution does not mimic the mean zonal velocity variation perfectly because of the mixed layer depth variation and the strong impact of eddy heat flux divergence. This is discussed further below.

In the EC region, 110°W-95°W, the contribution of zonal advection is always positive. The external heat flux and the zonal advection terms are balanced primarily by the vertical mixing whose amplitude exceeds 100 Wm^{-2} during late boreal summer when zonal advection is at its maximum. Vertical advection is also important, contributing to cooling of about 30-40 Wm^{-2} throughout the year. As in the CE region, lower surface heat flux, vertical entrainment, weak meridional advection and enhanced vertical mixing lead to the cooling tendency during boreal summer.

In the EE region, 95°W-85°W, the surface heat flux has a predominantly annual variation. Vertical advection and vertical mixing always make cooling contributions of comparable magnitude with largest values of about 50 Wm^{-2} during boreal spring. The role of horizontal advection is less significant in both runs but they differ in effect. In the late boreal summer/early autumn the P-FSU climatology shows a slightly larger warming tendency due to zonal advection and no significant effect of meridional advection. In the P-SSMI climatology zonal advection contributes to a very weak cooling tendency while the meridional advection contribution is stronger and has a warming tendency.

In the eastern Pacific it is necessary to distinguish between contributions to SST tendency by the low-frequency component of horizontal advection and the eddy advection related to the tropical instability waves (TIW) with wavelengths of 10°-12° just north of the equator (e.g. KRC). Low-frequency zonal advection is $\langle u \rangle \langle \partial T/\partial x \rangle$, where the brackets indicate low frequency filtering. In this analysis monthly averaged values were used so that $\langle u \rangle$ is the zonal velocity shown in figure 9. Since the TIW have periods of about 20 days, monthly averaging is barely adequate to discriminate the eddy effects of TIW variability. However, the results are consistent with those of KRC, so the interpretation does not seem to suffer

from this rather short averaging time scale. Eddy advection is the difference between the total zonal advection $\langle u\partial T/\partial x\rangle$ and the low-frequency component. Figure 13 shows the total heat flux due to zonal advection $Q_{zon.adv.} = -\rho_0 C_p\langle uh\partial T/\partial x\rangle$, the low frequency component $Q_{low-frq.} = -\rho_0 C_p\langle u\rangle\langle h\rangle\langle\partial T/\partial x\rangle$ and the eddy component $Q_{eddy} = Q_{zon.adv.} - Q_{low-frq.}$. Only three eastern regions are shown since in the western Pacific ocean eddy advection is negligible. In the CE region both $Q_{low-frq.}$ and Q_{eddy} are important, but are of opposite sign and nearly balance, especially for P-FSU. In the EC region the positive contribution by Q_{eddy} is clearly dominant, in good agreement with KRC who found that in 120°-90°W region eddy advection is most important during boreal summer and fall contributing to a warming tendency of SST while the low frequency component contribution is mainly a cooling tendency. In the EE region the $Q_{zon.adv.}$ and both eddy and low frequency components are generally small. P-FSU tends to have a stronger warming contribution in this region, almost 30 Wm^{-2}, due to $Q_{low-frq.}$ during late boreal summer.

The budget analyses above are fairly consistent with those computed by CBR. Their analysis regions were broader than those used here, and encompassed a broader meridional extent: 5°S-5°N, and the ocean model is, of course, different. CBR considered the effects of various thermodynamic processes directly on the evolution of $\partial T/\partial t$. By considering $\rho_0 C_p h\partial T/\partial t$ we include the impact of thickness variations. The factor of h does not affect the sign of the SST tendency, and it does not affect the relative contributions of various terms to this tendency, however h itself has a distinctly different seasonal cycle across the equatorial Pacific (see figure 9). Thus, although a quantitative comparison of the two studies is not feasible, the qualitative comparison is valid. Good agreement is found in the seasonal cycle of $\partial T/\partial t$, the external heat flux and the zonal advection term in all parts of the Pacific basin, but the estimates of the relative significance of the vertical mixing and vertical advection terms are different. The combined effect of the two processes is similar in both studies, but in contrast to Poseidon, the dominant role in the central and eastern basin in the Gent-Cane model used by CBR is played by the vertical advection term. Similar results

are given by KRC, who analyzed the mixed layer heat budget in the eastern Pacific using the same Gent-Cane model. In the EC region which is contained within the region analyzed by KRC we find that on average the amplitude of the vertical mixing contribution is at least twice as large as that of the vertical advection, while KRC study suggests that it is the vertical advection process that contributes more than the vertical mixing. Obviously, there are different implementations of bulk mixed layer dynamics and the differences in inferred entrainment rate must be compensated by differences in the estimates of the other diapycnal fluxes. However, the seasonal variation of the sum of these manifestations of diapycnal fluxes is similar in this study and in the work by KRC, with values of 70-90 Wm^{-2} in boreal spring and about 130 Wm^{-2} in boreal fall.

The study of the sea surface temperature variability in the eastern equatorial Pacific by Hayes et al. [1991] is based on the measurements taken at moorings at 110°W for the period 1986-1988. Their analysis indicates that "although no single process dominated SST change, the most important processes in the mean balance were the net incoming surface flux, the penetrative solar radiation, and the vertical turbulent flux out the bottom of the mixed layer". The magnitude of the vertical mixing term in the heat flux equation as estimated by Hayes compares well with Poseidon values, while in the KRC analysis it is much smaller. It should be noted that estimates of vertical advection are difficult to infer from observations. However, the estimates derived from the Poseidon model are in good agreement with observational estimates of the terms of mixed layer heat budget.

4. Variations during 1994-1995

4.1. Wind Stress and Current

As can be readily observed in the WW region zonal wind stress, τ_x, was weakening during most of 1994 until the westerly burst of December 1994. In 1995 easterly zonal wind stress was stronger than usual starting in early boreal spring through to the end of the year.

Meridional wind stress was about normal in 1994 and weaker in 1995. In the WC region zonal wind stress weakened throughout 1994 and increased during 1995 always preserving its easterly direction. Meridional wind stress was close to climatology. In the CW region a reduction in zonal wind stress occurred during boreal fall in 1994. During 1995 SSMI zonal wind stress was weaker than FSU. Meridional wind stress was close to climatology in this region. In the CE region, the FSU zonal wind stress was also slightly stronger than that from SSMI, especially during boreal summer in 1994 and throughout 1995. The SSMI meridional wind stress was weaker than usual in late boreal spring/summer, and FSU from spring through fall during both years. In the EC region, the FSU zonal wind stress was also slightly stronger than SSMI and climatology during boreal summer and fall 1994. The SSMI meridional wind stress was weaker than normal during the entire 2-year period except for boreal winter 1994-1995. The FSU meridional wind stress was close to climatology. In the EE region zonal wind stress was close to climatology and SSMI meridional wind stress was weaker than climatology.

Anomalous variations of zonal velocity, u, are characterized in the western Pacific (WW and WC regions) by stronger than normal eastward current during boreal spring and summer 1994 and in December 1994 (figure 9). Westward flow returned in early 1995 and was stronger than usual throughout the year. In the CW region the zonal current was near normal during 1994 but westward flow was slightly stronger during late boreal winter/early spring and early fall 1995. Less agreement was found regarding the details of zonal velocity evolution between the two simulations in the eastern basin (EC, CE and EE). P-FSU shows much stronger than usual eastward current during boreal spring 1994 in these regions whereas P-SSMI is anomalous only in the EE region. Both simulations tend to show anomalous westward flow during boreal winter 1994-95.

4.2. Mixed Layer Depth

During 1994-95 the MLD anomalies rarely exceeded 10 m. Changes in meridional convergence or vertical entrainment in response to wind anomalies were usually mutually compensating. The MLD anomalies were due to small imbalances between these terms and, less frequently, enhancement of zonal convergence (particularly in the WC and CW regions during winter 1994-95).

4.3. SST Tendency

This section contains the detailed analysis of the influence of various terms in the surface heat budget and the processes responsible for SST anomalies during 1994-1995. Only features present in both P-FSU and P-SSMI simulations are discussed, aiming for consistency in explaining the warming event.

The analysis in this section is based on the inspection of time series of various terms in heat budget summarized in figure 12 with the aid of zonal velocity and mixed layer depth series in figure 9.

WW: 155°E-175°E

Beginning in March 1994 there was an enhanced warming tendency due to stronger heating and weaker vertical diffusion. Zonal advection, although contributing strongly to the cooling tendency in the beginning of the year, started to increase SST in May when the warming tendency was the largest. From this time through November 1994 the surface temperature was above normal. In October 1994 zonal advection in P-FSU was warming SST but in P-SSMI its impact on SST tendency was very small. In the climatological annual cycle, zonal advection tends to cool SST at this time. By December 1994, zonal advection again contributed to the cooling tendency. This cooling was correlated with very low, even negative values of the external heat flux. Warming in the beginning of 1995 came earlier than usual but was very short lived. The anomalous warming was due to zonal advection in

P-SSMI and zonal and meridional advection in P-FSU which was different from climatology. By the end of 1994 the highest temperatures were observed to the east of the WW region (figures 5 and 6). Acting on this temperature gradient, the strong westward current advected heat into the region. From April through the end of 1995, the two hindcasts did not always agree on the sign of $\partial T/\partial t$, which fluctuated rapidly but with small amplitude.

WC: 175°E-165°W

In this region the SST anomaly was the largest. As in the WW region, enhanced warming started in March 1994. In this region the warming lasted through November 1994 and was due primarily to enhanced external heat flux, related to the impact of weaker winds on the latent heat flux. During boreal fall 1994 the mixed layer was shallower than normal, winds were weaker than at any other time during the 2-year period, particularly in the zonal direction, so vertical mixing and zonal advection contributed less than usual to the cooling tendency. The cooling started in December 1994 and lasted at least through March 1995. Subsequently the simulations differ in the sign of $\partial T/\partial t$. The beginning of the cooling period coincided with a minimum of the external heat flux term, which was negative during winter 1994-95. Once the cooling began zonal advection contributed strongly to the cooling tendency. This large transport of the heat flux by the zonal advection was associated with anomalous intensification of the westward current acting on the climatological thick mixed layer in February - April 1995 (figure 9). With lower SST east of the WC region (figures 5, 6), zonal advection continued to cool the surface during boreal spring.

CW: 165°W-145°W

As in the WW and the WC regions, the sea surface temperature tendency is strongly correlated with the external heat flux term in this region and has a strong semiannual component. In boreal spring 1994 the warming tendency was stronger than usual due to stronger external heating. The cooling tendency in late summer was close to climatology although the relative contribution of various processes was different: cooling tendency of zonal advection was much stronger than usual and counteracted the effect of weaker than normal

vertical mixing and vertical advection as well as small warming tendency by meridional advection. The warming during boreal autumn early winter 1994 was associated with weaker zonal advection in P-SSMI and weaker vertical mixing in P-FSU. As in the WC region, the easterly wind stress was weaker than normal prior to the onset of cooling in November 1994, but as it rapidly regained its strength the cooling began. When the wind stress weakened the mixed layer shoaled but deepened again in response to the wind strengthening. Acting on a deep mixed layer, zonal advection continued to cool the surface during boreal spring 1995, delaying the spring warming for at least a month. Anomalous wintertime cooling was sufficient to overcome the prior warming so that during the remainder of 1995 the SST was lower than normal.

CE: 145°W-110°W

The warming in early 1994 was stronger and lasted longer than usual due to enhanced external heating and stronger warming tendency of zonal advection. These tendencies were partially compensated by enhanced vertical diffusion and meridional advection. The cooling tendency of vertical mixing decreased significantly towards the end of this warming period, thus allowing for its extended duration. But in this region the previous year was anomalously cold, so the effect of this enhanced warming was the return of SST close to climatological values. The cooling during June - August 1994 had magnitude similar to climatology: the strong cooling tendency of zonal advection was compensated by weaker vertical mixing. In boreal autumn of 1994 a strong warming in SST was related to much weaker vertical mixing. Vertical mixing was still weak during December - January when anomalous cooling was due to zonal advection and low external heat flux. Note that the cooling tendency of zonal advection in autumn 1994 was opposite to its usual effect. This happened at a time when the monthly mean zonal current was either normal (P-FSU) or weaker than normal (P-SSMI) and the mixed layer deeper than usual. The effect may be traced to the reduction in TIW activity and reduction in the meridional gradient north of the cold tongue during this time (figure 13) particularly in the P-SSMI simulation. In P-SSMI the cooling was more

extensive since the mixed layer stayed deeper than usual for a longer period of time. As a result, the warming in the beginning of 1995 came later than usual. In P-FSU the warming in the beginning of 1995 was also weaker than in 1994 due to an increased cooling tendency of vertical mixing. During the second half of 1995 SST decreased more rapidly than usual. Note that the two model runs did not always agree on details of SST evolution, except for an enhanced cooling tendency of vertical mixing.

EC: 110°W-95°W

The SST in P-SSMI was about 2°C lower than normal at the start of the study period. During the first two months of 1994 although the external heating was stronger than usual, the cooling tendency of vertical mixing was also enhanced, so that only a slight warming resulted. In the P-FSU simulation the warming lasted for about 5 months, and decrease in external heating was matched by weakened vertical mixing. In P-SSMI the cooling tendency of vertical mixing and vertical advection was stronger during the same months, so the overall increase in SST was smaller and the SST anomaly remained negative. The cooling during boreal summer 1994 was due to diminished external heating and weakened warming tendency by zonal advection. This changed to warming in October 1994 similar to climatology and there was no successive change to anomalous cooling as in the regions to the west. The SST in P-SSMI returned to normal by August 1995, much later than in P-FSU for which the anomaly was quite small (<0.5°C) over most of the study period. From December 1994 through spring 1995 the SST tendency was small and fluctuating, so there was little consensus between model runs. After June 1995 the SST evolution was close to climatology and the model simulations are in closer agreement.

EE: 95°W-85°W

The amplitude of $\partial \mathrm{SST}/\partial t$ was relatively small in this region, particularly in the P-FSU hindcast, and there were differences in the details of $\partial \mathrm{SST}/\partial t$ evolution between the two model runs. Overall, there was a net cooling during the first half of 1994 and warming during the second half of the year. The P-FSU simulation was close to climatology in June

- December 1994. In P-SSMI we observe stronger warming in late autumn and early winter 1994 (in spite of lower than usual external heating) due to stronger warming tendency by meridional advection and reduced vertical advection and vertical mixing. As in the EC region, in the second half of 1995 the more typical behavior was observed in both model runs.

5. Discussion and Summary

The 1994-1995 warming event was of a small amplitude relative to the large El Niños of 1982-1983 and 1997-1998 and never developed into a strong El Niño. Yet, it was very well observed and the sea surface temperature evolution could be analyzed in detail. For significant changes in SST, AVHRR and TAO data sets show good agreement. Some discrepancies are due to spatial resolution, since in the case of AVHRR a spatial average of data was considered while for TAO measurements were available only at pointwise locations so that the effects of local processes were not smoothed out, particularly in the eastern basin, where the spatial correlation scales are quite short. The analysis of the sign of $\partial \mathrm{SST}/\partial t$ shows that model performance compared with data was better with SSMI forcing. In the east, however, the ocean model underestimates the amplitude of SST variations thus making it more difficult to study this region where SST variations are highly sensitive to small details in forcing. The *Harrison et al.* [1990] analyses based on different wind products diverged in the western basin, and they could not discriminate between mechanisms forcing SST change. In contrast, in the present study it was found that the SST changes and the dominant terms in the heat budget are quite consistent in the western basin, although the amplitudes are small.

The climatological annual cycle of SST tendency in the western basin exhibits a strong semiannual signal, dominated by the external heating of moderate magnitude. In the central basin the external heating is stronger and so is the magnitude of other terms in the heat

budget. A complicated balance is inferred, with horizontal advection, vertical mixing and vertical advection contributions being of comparable strength. In the eastern basin SST tendency is dominated by the external heating and vertical mixing, both of which have a strong annual signal. The magnitude of the dominant terms in the heat budget increases from west to east. External heat is largest in 145°W-110°W (CE) and 110°W-95°W (EC) regions, where it exceeds 100 Wm^{-2} while near the western boundary it is less than 50 Wm^{-2}. Near the eastern boundary (95°W-85°W (EE) region), vertical advection is as important as vertical diffusion.

The warming in the western equatorial Pacific (WW: 155°E-175°E and WC: 175°E-165°E) during most of 1994 was related to the diminished surface wind stress. This led to reduction in the advective influence on the sea surface temperature and to an increase in the external heat flux in the beginning of the year. The winds steadily diminished in the western basin throughout 1994, leading to a reduction in the intensity of all processes that usually contribute to cooling tendency: vertical advection, vertical mixing and horizontal advection. High SST and weak winds led to a reduction in external heating, and in December 1994 surface cooling began and was more intense and lasted longer than usual. The dominant process in this cooling was zonal advection: in December 1994 a strong eastward current acted on a positive zonal temperature gradient because of localized warming within the warm pool and cooling to the west (see figures 4-6). This was replaced in January - March 1995 by a strong westward current and negative zonal temperature gradient. During the rest of 1995 the westward wind stress was stronger than normal, the mixed layer stayed slightly deeper than usual and thus the cooling tendency of zonal advection was enhanced. This led to the negative SST anomaly towards the end of 1995 consistent with observed cooling event in 1995-1996 (figure 3).

In the central Pacific (CW: 165°W-145°W), with establishment of a large positive SST anomaly in the WC region, a strong negative temperature gradient developed during 1994, so that the westward current contributed significantly to cooling in December 1994. Throughout

boreal winter and spring of 1995 zonal advection, acting on a deeper than normal mixed layer, was cooling the surface. By the end of 1995 the cold SST anomaly reached 1°C.

The composition of the mixed layer heat budget is very different in the western and eastern Pacific, so the CE region has a transitional nature, with all the terms contributing significantly to the SST tendency. In this region enhanced external heating and reduced vertical mixing in the beginning of 1994 helped restore SST to normal following the anomalously cold conditions of 1993. These processes were aided by a slightly stronger than usual warming zonal advection tendency. During the first three months of 1994 this was related to enhanced activity of eddy processes. In April - May the strengthening of $Q_{zon.adv.}$ was due to stronger than normal eastward mean zonal current, especially in P-FSU (figure 9). During the second half of 1994 the enhanced zonal advection cooling tendency was due to the mean flow acting on a deeper than normal mixed layer, while the eddy term was either normal (in P-FSU) or weaker than usual (in P-SSMI) (figure 13). However, this cooling tendency was compensated by weaker than usual cooling tendency of vertical mixing. *Hayes et al.* [1991] found that the Richardson number tends to be large when the mixed layer is deep and high Ri suppresses the turbulent flux. In the beginning of 1995 when the SST anomaly was small the two model simulations did not always agree on the details of the SST evolution. However, they agree well on that there was a cooling during boreal summer of 1995 due to enhanced vertical mixing which marked the end of the warming event.

In November - December 1994 the eastern Pacific SST was only slightly warmer than normal. However, the preceding year and the following year were colder than usual, so net warming occurred during 1994 and net cooling during 1995 in the eastern basin. In early 1994 enhanced surface heating and zonal advection warming tendency helped restore SST to its climatological values. In the EC region zonal advection contribution was dominated by eddy processes and Q_{eddy} was larger than usual at this time. During late 1994 a stronger than usual warming occurred. This warming, while was more apparent in the P-SSMI simulation, was due to a reduced cooling tendency in vertical mixing and vertical advection associated

with a deeper than normal mixed layer. During the first half of 1995 the export of heat from the surface layer due to entrainment and vertical mixing slowly strengthened with the strengthening wind stress, until June 1995 after which cooling occurred.

In the easternmost Pacific ocean (the EE region) SST remained colder than usual until the beginning of boreal autumn 1994. In this region vertical mixing and vertical advection were the dominant contributors to the cooling tendency. This terms were strongly correlated with each other and with variations in the mixed layer depth.

During 1994-1995 the largest positive SST anomalies were observed in the mid-basin and was associated with reduced latent heat flux due to weak surface winds. In contrast, during the 1982-1983 El Niño, the SST anomaly was largest in the eastern basin and *Harrison et al.* [1990] show that the anomaly was due to zonal advection rather than anomalous surface heat flux.

The results in the eastern basin agree with the conclusions of *Harrison et al.* [1990], who found that during 1982-1983 El Niño zonal advection was the major surface warming factor between 160°W and 130°W. For the region 120°W-110°W, their hindcasts using different wind products were not consistent in terms of a dominant mechanism for SST warming. This is not surprising since this location lies within the CE region where several processes were equally important. The same applies to the region from 100°W-90°W, which roughly corresponds to the EE region. Just as in their study of the 1982-1983 El Niño, a cooling tendency was manifest in Poseidon hindcasts during June - July 1995 throughout the entire equatorial Pacific (with the exception of the WW region), signaling the end of the warming event. Harrison et al. attributed the onset of this cooling to the return of easterlies and to strengthening of the easterly wind stress in the mid-basin. During the 1994-1995 a reversal of the zonal wind component was almost never observed, undoubtedly helping to explain why the 1994-1995 event was weak. The initiation of cooling in mid-1995 was timed with the increase in easterly wind stress in the western and central basin (WC, CW and CE regions) and, just as Harrison et al. suggested, once the cooling had begun in response to reduced

surface heating, horizontal advection began to enhance the cooling tendency. In the eastern equatorial Pacific enhanced diapycnal mixing, primarily vertical diffusion, but also vertical entrainment, was the dominant mechanism responsible for the cooling during the summer 1995.

The analysis of a relatively low amplitude warming event became possible due to availability of fine resolution surface temperature data and a skillful ocean model. Certain limitations, however, still remain. In particular, the sensitivity of the model heat budget to the wind stress, especially in the eastern parts of the Pacific ocean, indicates the need for better wind stresses as were available for a short period from NSCAT [*Bourassa et al.*, 1997]. High quality surface flux products remain one of the highest priorities for helping us understand ocean variability even at seasonal to interannual time scales.

Acknowledgments. The study was supported by funding provided by NASA Physical Oceanography Program under RTOP 622-24-48 and computer time and assistance by the NASA Center for Computational Sciences at Goddard. We thank the following people and organizations for providing their datasets for the study: NOAA/PMEL for TAO data, K. Casey for processing the AVHRR Pathfinder data which was originally provided by the JPL PODAAC, R. Atlas and J. V. Ardizzone for the wind product based on SSM/I data, R. Reynolds for the blended FSU/NCEP wind stress analysis.

References

Atlas, R., Bloom, S. C., Hoffman, R. N., Ardizzone, J. V., and Brin, G. Space-based surface wind vectors to aid understanding of air-sea interactions. *Eos, Transactions, Amer. Geophys. U.*, 72:201,204,205 and 208, 1991.

Bourassa, M. A., Freilich, M. H., Legler, D. M., W.Timothy, and O'Brien, J. wind observations from new satellite and research vessels agree. *Eos, Transactions, Amer. Geophys. Un.*, 78(51):597, 602, 1997.

Casey, K. S. and Cornillon, P. A comparison of satellite and in situ based sea surface temperature climatologies. *J. of Clim.*, 12(6):1848–1863, 1999.

Chen, D., Busalacchi, A. J., and Rothstein, L. M. The role of vertical mixing, solar radiation, and wind stress in a model simulation of the sea surface temperature seasonal cycle in the tropical pacific ocean. *J. Geophys. Res.*, 99:20,345–10,359, 1994.

Harrison, D. E., Giese, B. S., and Sarachik, E. S. Mechanisms of SST change in the equatorial waveguide during the 1982-83 ENSO. *J. Clim.*, 3:173–188, 1990.

Harrison, E. F., Minnis, P., Barkstrom, B., and Gibson, G. Radiation budget at the top of the atmosphere. In Gurney, R. J., Foster, J. L., and Parkinson, C., editors, *Atlas of satellite observations related to global change*, pages 19–38, 1993.

Hayes, S. P., Chang, P., and McPhaden, M. J. Variability of the sea surface temperature in the eastern equatorial pacific. *J. Geophys. Res.*, 96:10553–10566, 1991.

Kalnay, E. and coauthors. The ncep/ncar 40-year reanalysis project. *Bulletin of the Amer. Meteorol. Soc.*, 1996.

Kessler, W. S., Rothstein, L. M., and Chen, D. The annual cycle of SST in the eastern tropical Pacific, diagnosed in an ocean GCM. *J. Clim.*, 11:777–799, 1998.

Köberle, C. and S.G.H.Philander. On the processes that control seasonal variations of sea surface temperatures in the tropical pacific ocean. *Tellus*, 46A:481–496, 1994.

Kraus, E. B. and Turner, J. S. A one-dimensional model of the seasonal thermocline. ii: The general theory and its consequences. *Tellus*, 19:98–109, 1967.

Large, W. G. and Pond, S. Open ocean momentum flux measurements in moderate to strong winds. *J. Phys. Oceanogr.*, 11:324–336, 1982.

McPhaden, M. J. and coauthors. The tropical ocean-global atmosphere (toga) observing system: A decade of progress. *J. Geophys. Res.*, 103:14169–14240, 1998.

Pacanowski, R. and Philander, S. G. H. Parametrization of vertical mixing in numerical models of tropical oceans. *J. Phys. Oceanogr.*, 11:1443–1451, 1981.

Rossow, W. B. and Schiffer, R. A. Isccp cloud data products. *Bull. Am. Met. Soc.*, 72:2–20, 1991.

Schopf, P. S. and Loughe, A. A reduced-gravity isopycnal ocean model: Hindcasts of El Niño. *Mon. Weath. Rev.*, 3(9):2839–2863, 1995.

Seager, R., Blumenthal, M. B., and Kushnir, Y. An advective atmospheric mixed layer model for ocean modeling purposes: Global simulation of surface heat fluxes. *J. Clim.*, 1994.

Shapiro, R. Smoothing, filtering and boundary effects. *Rev. of Geophys. Space Phys.*, 8(2):359–387, 1970.

Xie, S.-P. On the genesis of the equatorial annual cycle. *J. Clim.*, 7:2008–2013, 1994.

Yang, S., Lau, K.-M., and Schopf, P. S. Sensitivity of the tropical Pacific Ocean to precipitation-induced freshwater flux. *Climate Dynamics*, 15:737–750, 1999.

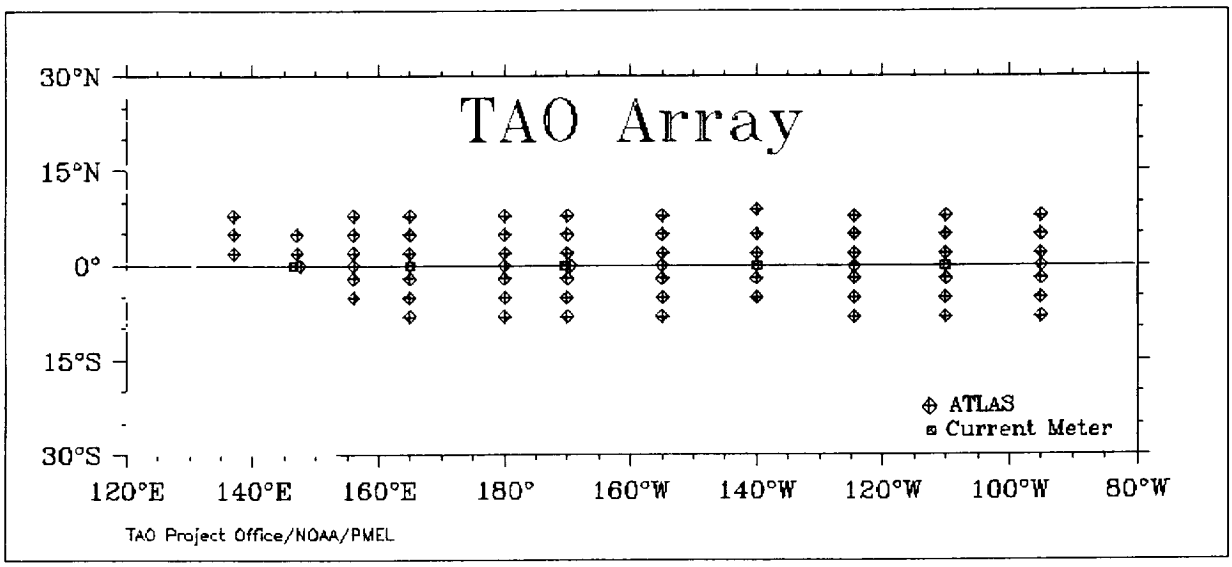

Figure 1: Map of the TAO array, consisting of approximately 70 moored ocean buoys in the Tropical Pacific Ocean. This figure is obtained through the TAO Web Page http://www.pmel.noaa.gov/toga-tao/home.html

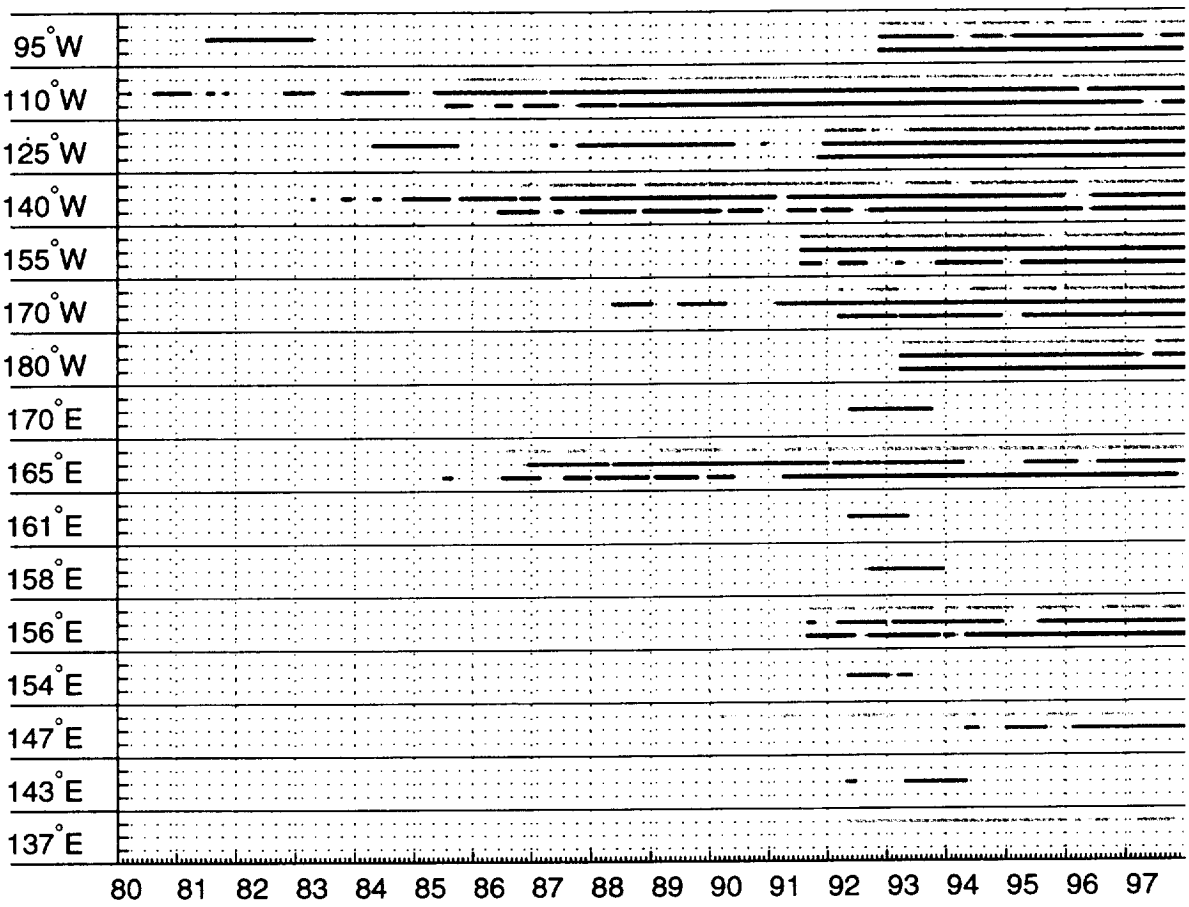

Figure 2: Availability of SST data from TOGA TAO array in the equatorial region during 1980-1997. For each longitude the periods of available records from the three buoys spanning the equator are shown: top (light) line at 2°N, middle (medium darkness) line at equator and bottom (dark) line at 2°S.

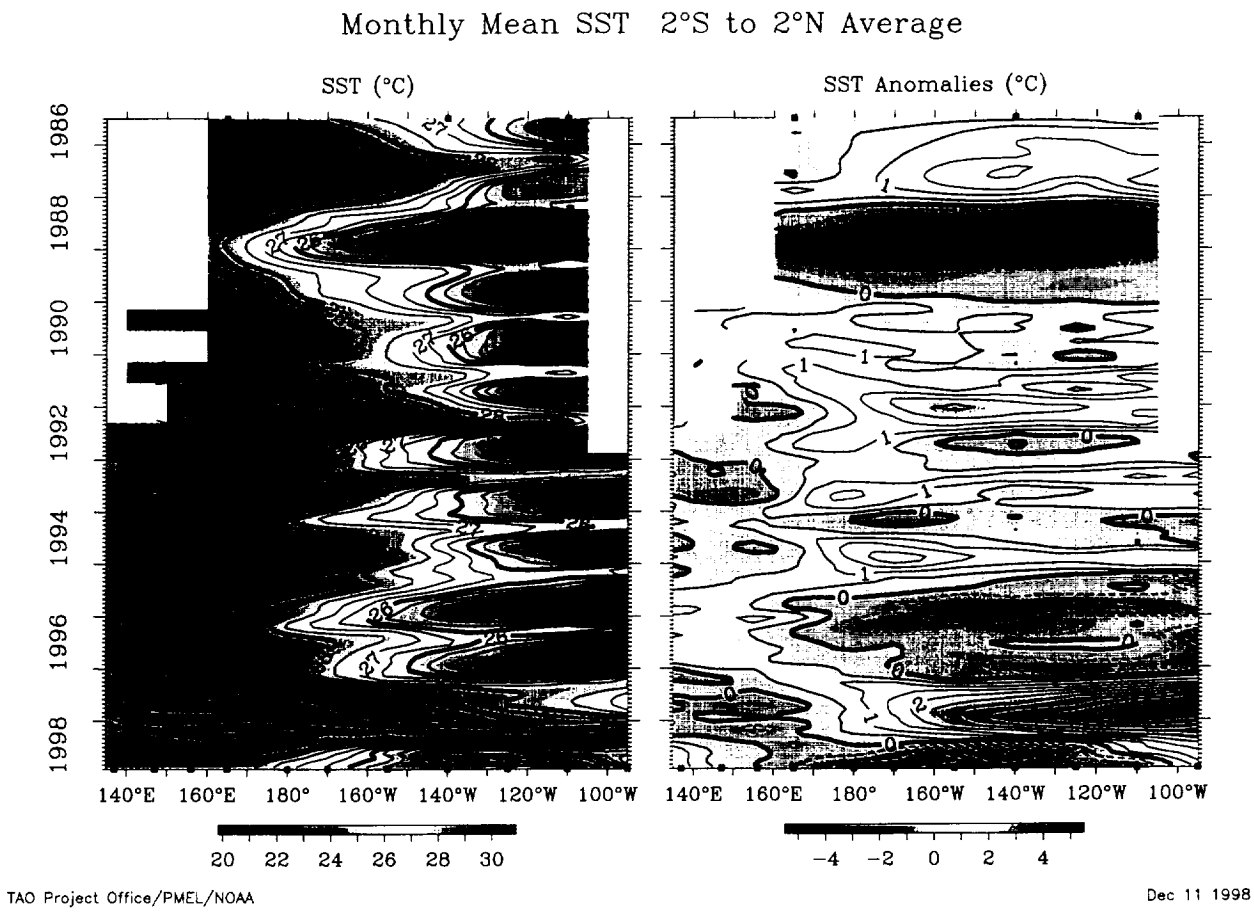

Figure 3: Evolution of SST based on the analysis of the observations by TOGA TAO moorings. This figure is obtained through the TAO Web Page http://www.pmel.noaa.gov/toga-tao/home.html

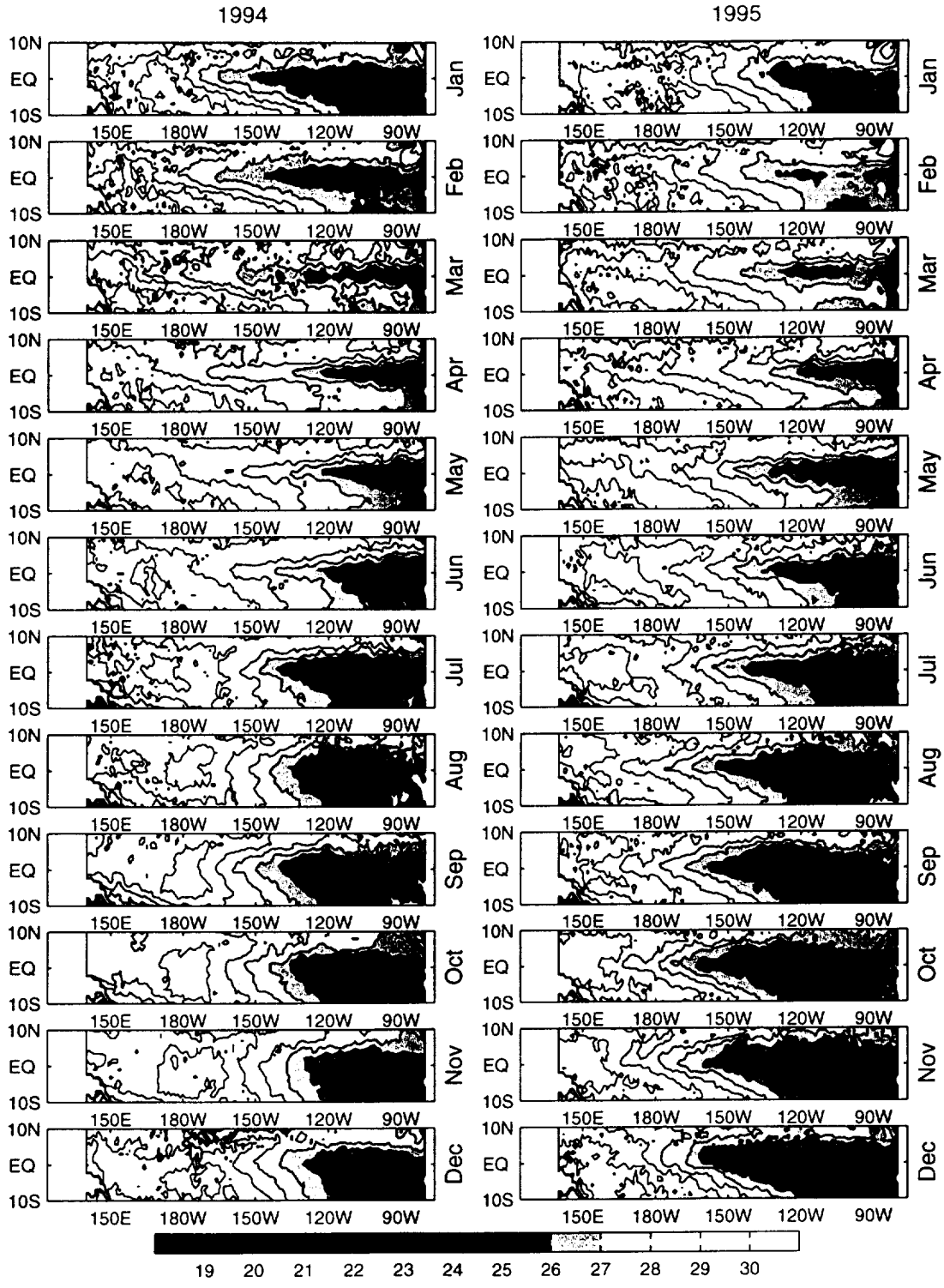

Figure 4: Evolution of SST based on the analysis of the Pathfinder AVHRR data. White areas are due to missing data, generally related to persistent cloudiness in the region.

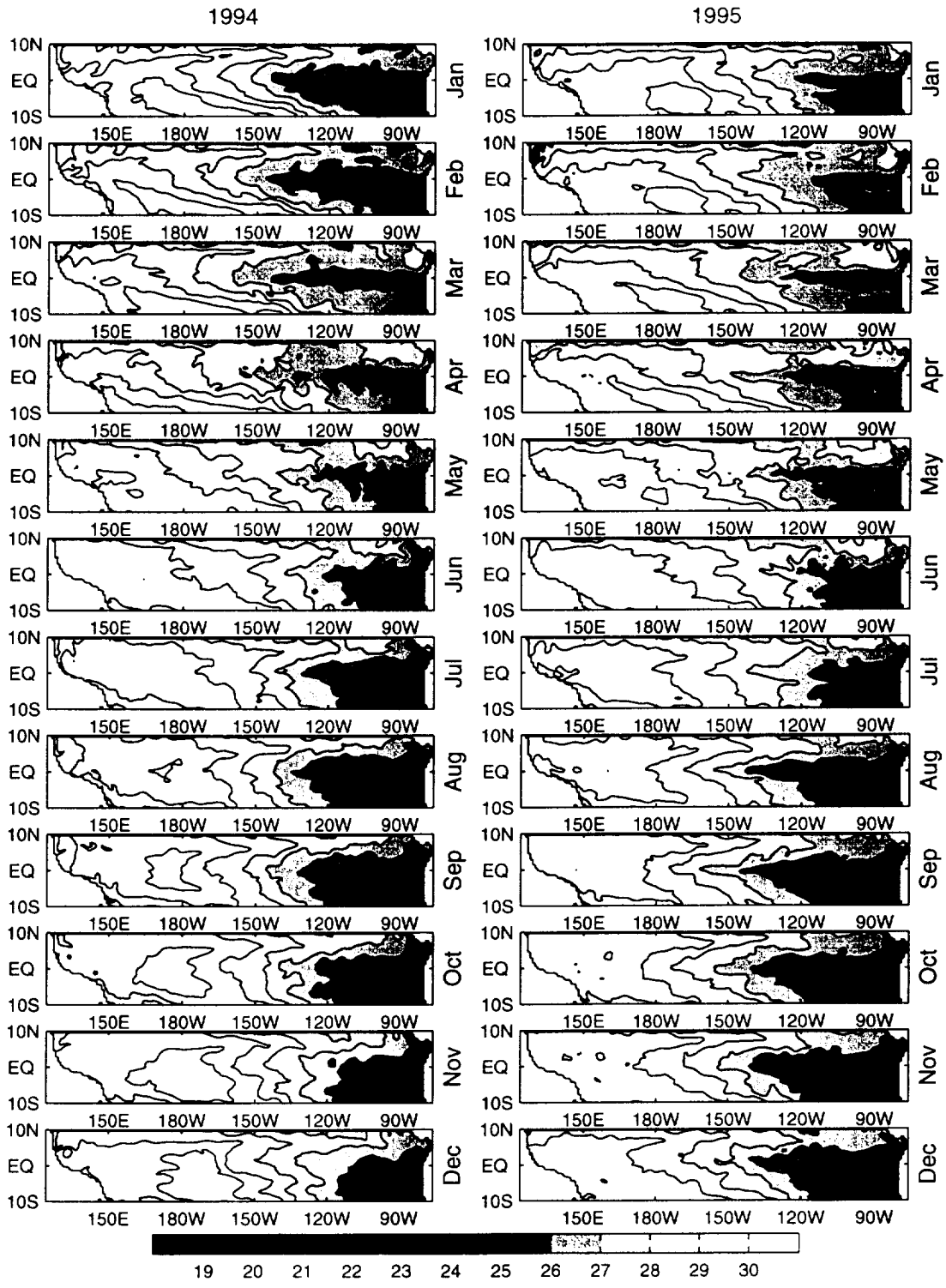

Figure 5: Evolution of SST simulated by the Poseidon model forced with SSMI winds.

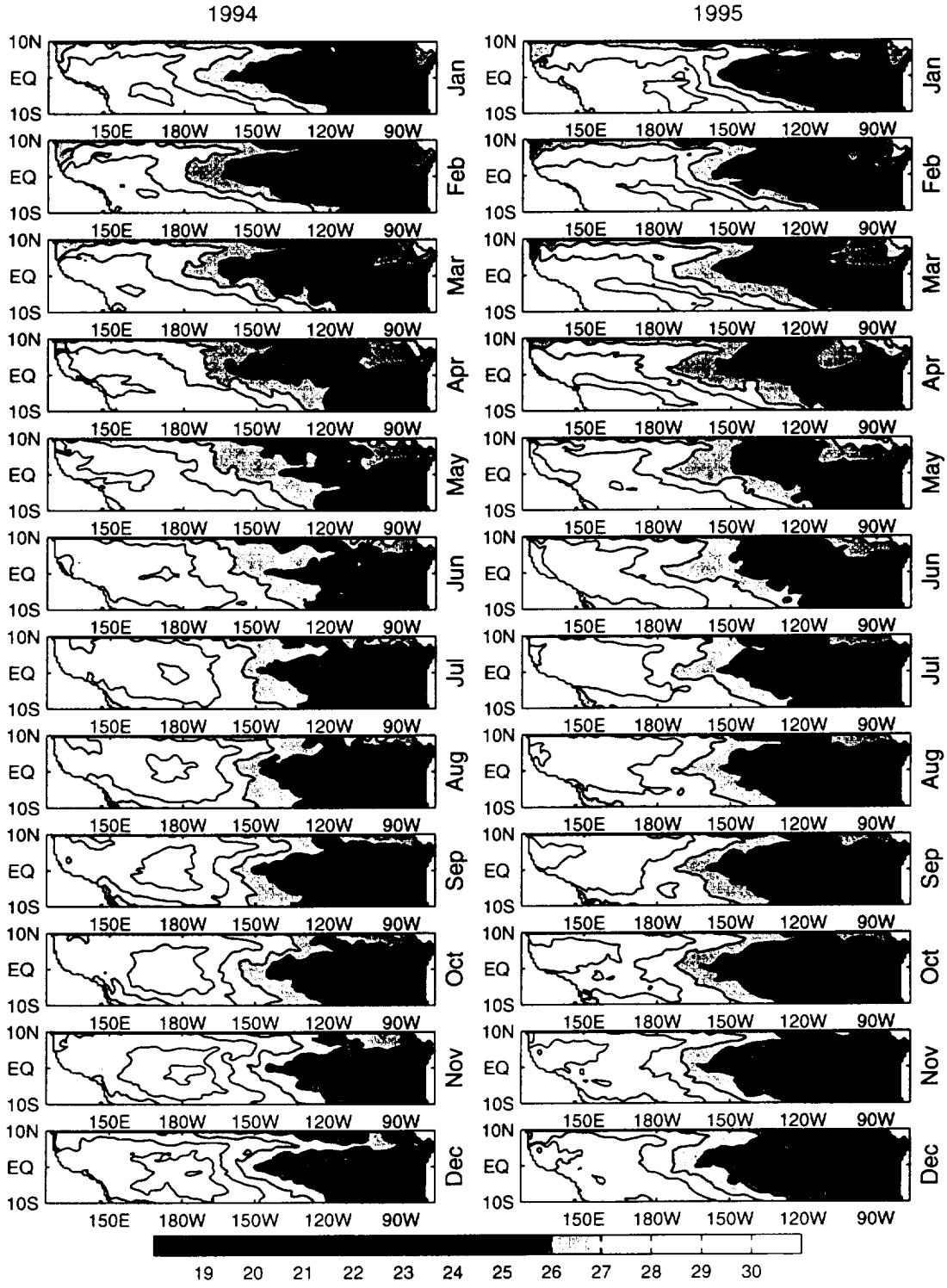

Figure 6: Evolution of SST simulated by the Poseidon model forced with FSU winds.

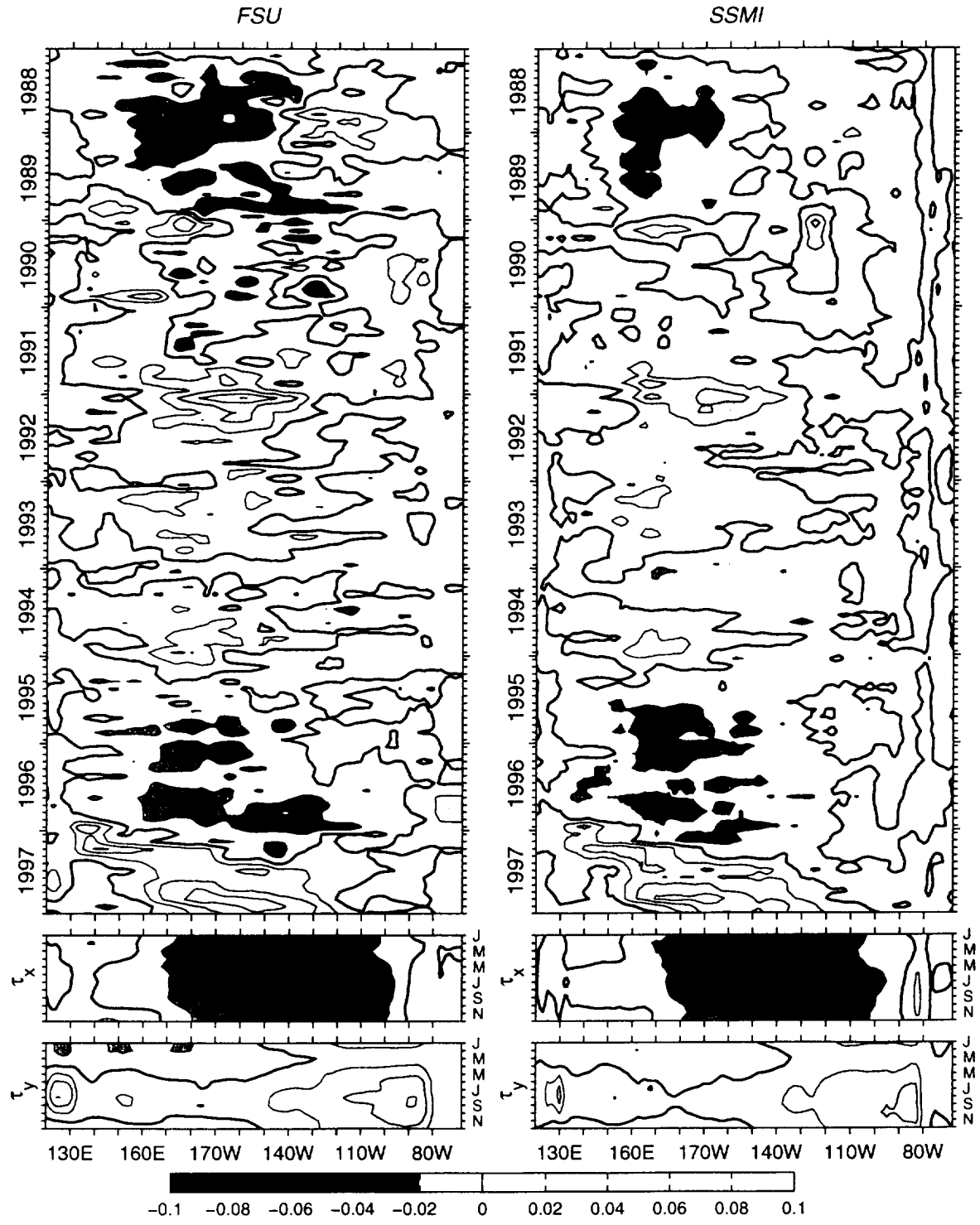

Figure 7: Top panel: zonal wind stress in Nm^{-2} anomaly for 10-year period. Lower small panels: climatology of FSU and SSMI zonal and meridional wind stress components based on data from 1988-1997 period.

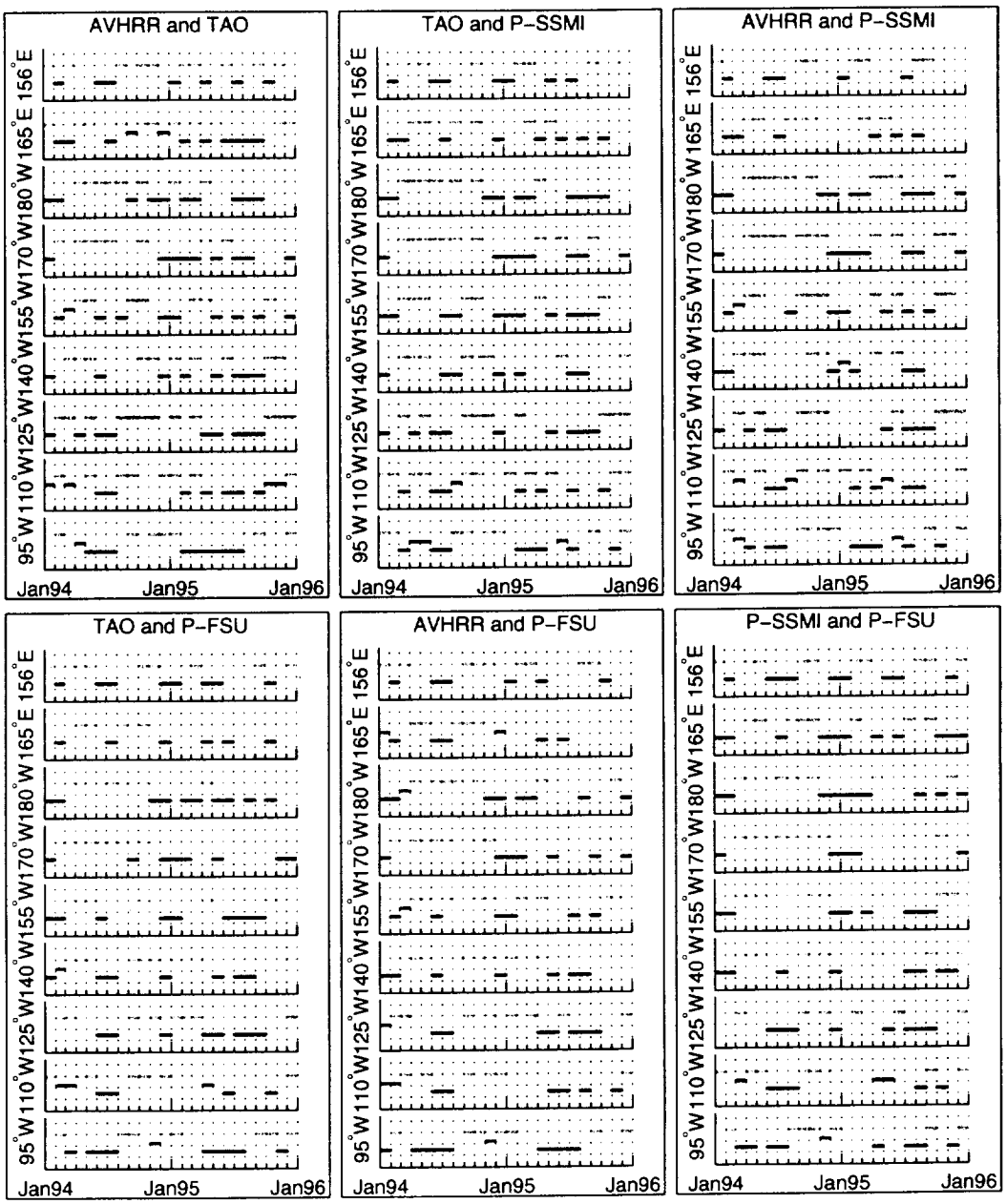

Figure 8: Agreement in sign of $\partial SST/\partial t$ between data and model output as well as between two datasets and two model runs. Only values of $|\partial SST/\partial t|$ >0.5°C/month are considered. For each longitude top (light) line indicates warming, middle (medium darkness) line shows periods of diagreement and bottom (dark) line cooling. All fields are averaged in time over a month. The space average is taken over boxes of size 5° in longitude by 4° in latitude centered at TOGA TAO coordinates along the equator. For TAO data the average is taken over three locations along the same latitude spanning the equator.

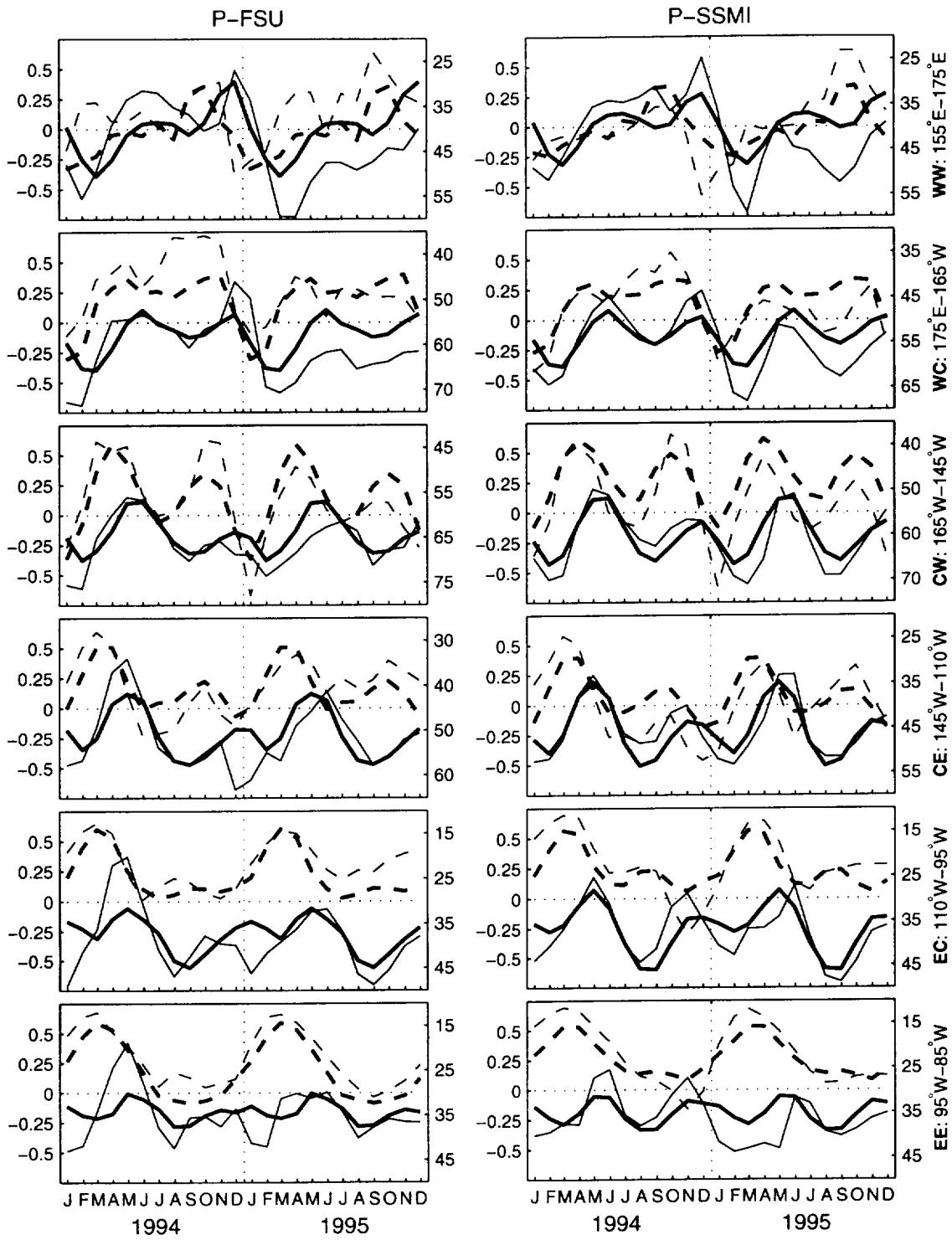

Figure 9: Zonal velocity in m/s (scale is on the left) and monthly means of mixed layer depth in m (scale is on the right). Thick lines show the climatologies. Dashed lines show the mixed layer depth and solid line the zonal velocity. The analysis regions correspond to those in figures 11 and 12. All fields are averaged in space the same way as in figures 11 and 12 . Note the different ranges of mixed layer depth for different analysis regions and for different model runs.

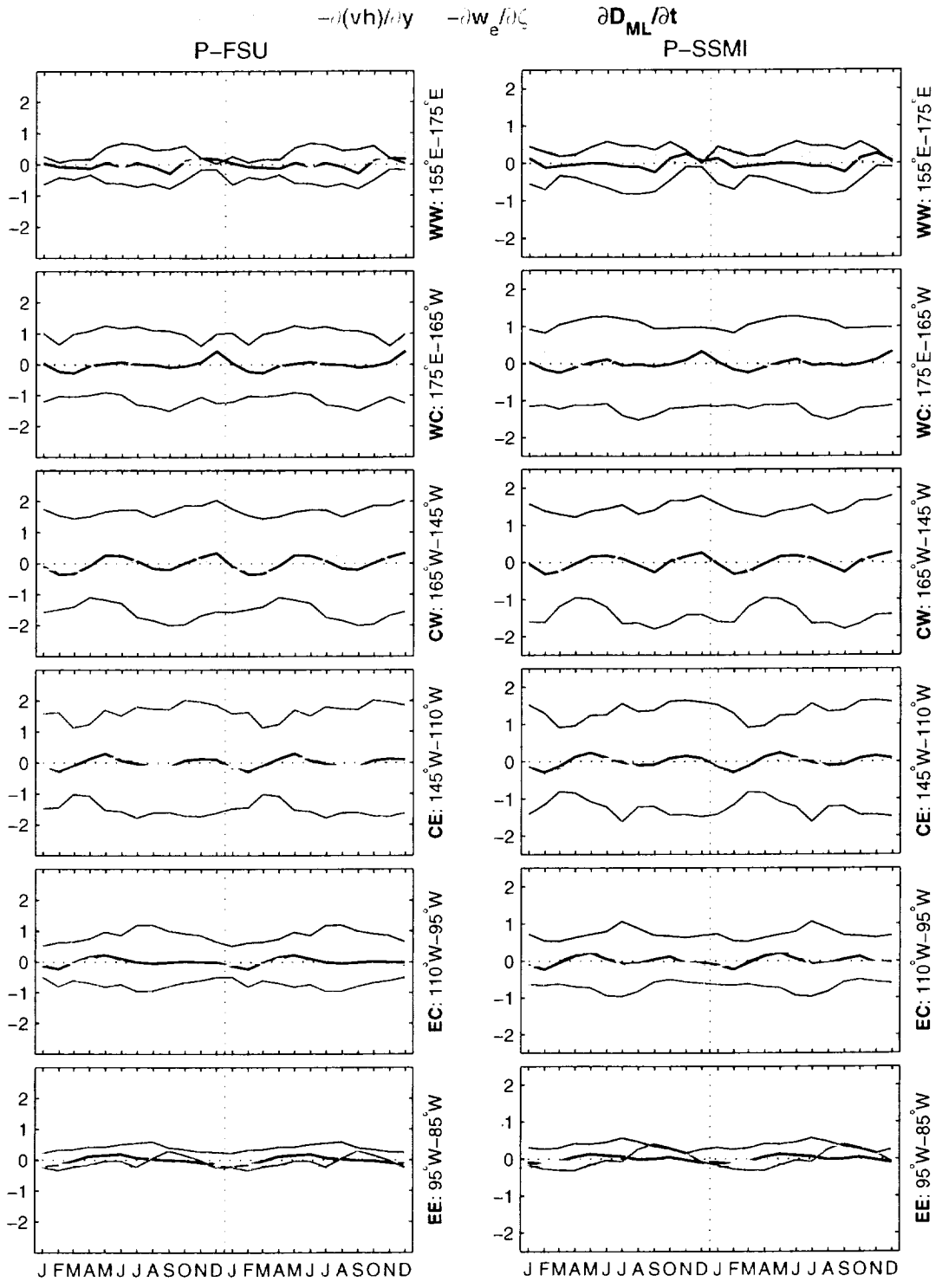

Figure 10: Climatological balance of terms (monthly means, units are m/day) in the continuity equation as derived from the model output. Two years are displayed for easy cross-reference with other figures. Spatially data was averaged over regions extending between indicated zonal limits and between 2°S and 2°N in latitude.

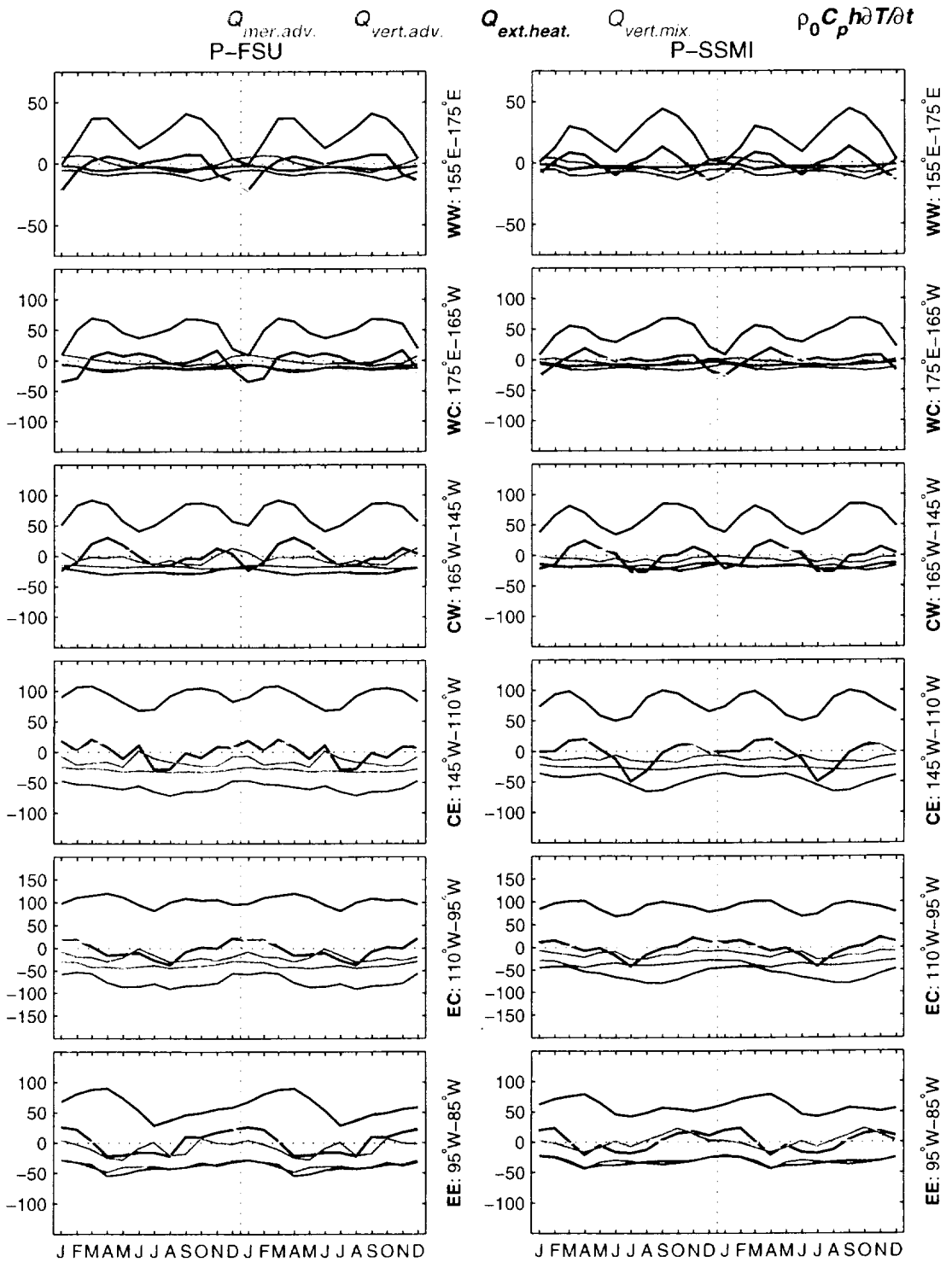

Figure 11: Climatological balance of terms (in Wm^{-2}) in the surface heat budget as derived from the model output. Two years are displayed for easy comparison with figure 12. Spatially data was averaged over regions extending between indicated zonal limits and between 2°S and 2°N in latitude. Note the different scales for different analysis regions.

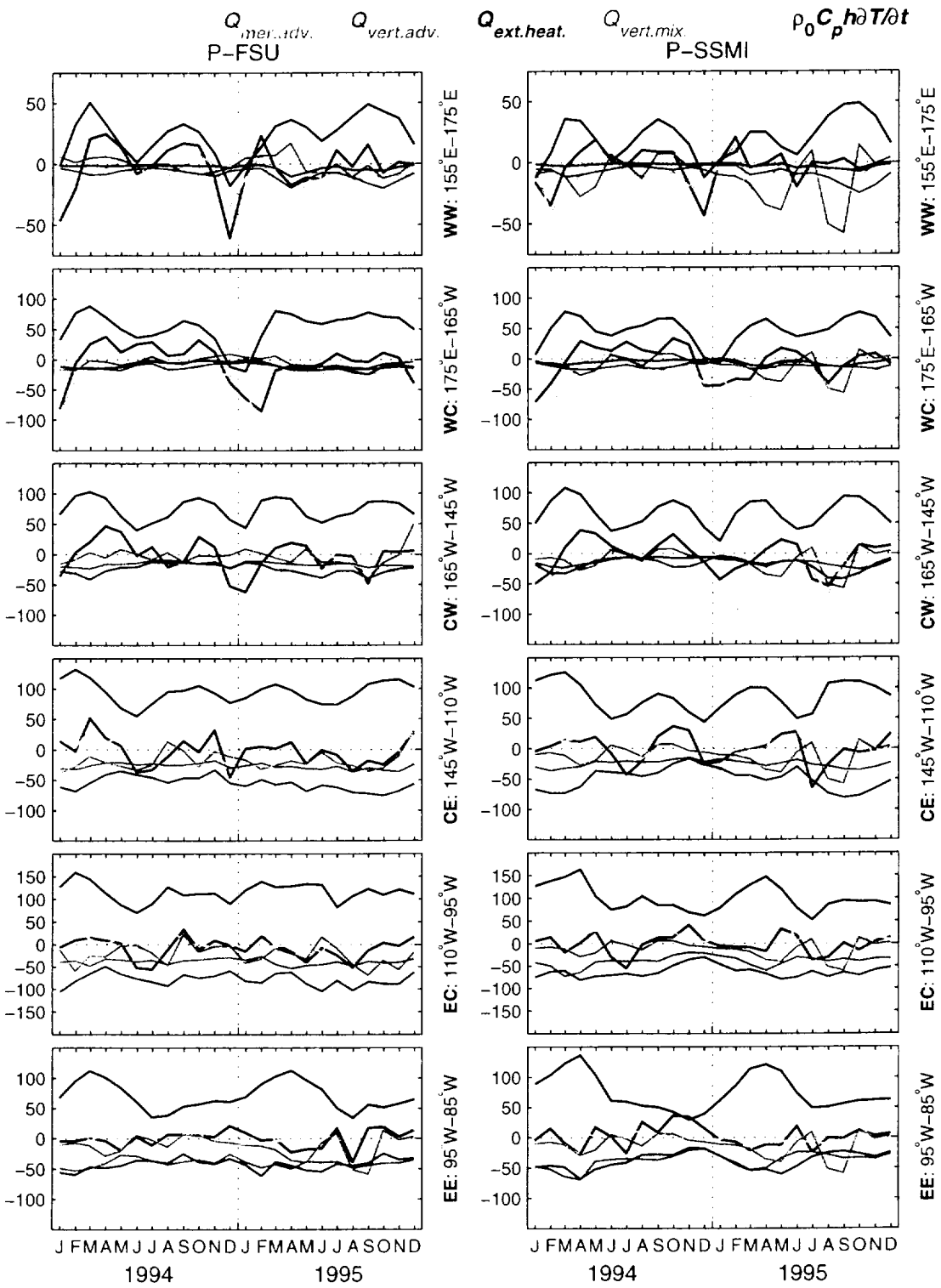

Figure 12: Balance of terms (in Wm^{-2}) in surface heat budget as derived from the model output. Each time series represents data averaged over regions extending between indicated zonal limits and between 2°S and 2°N in latitude. Note the different scales for different analysis regions.

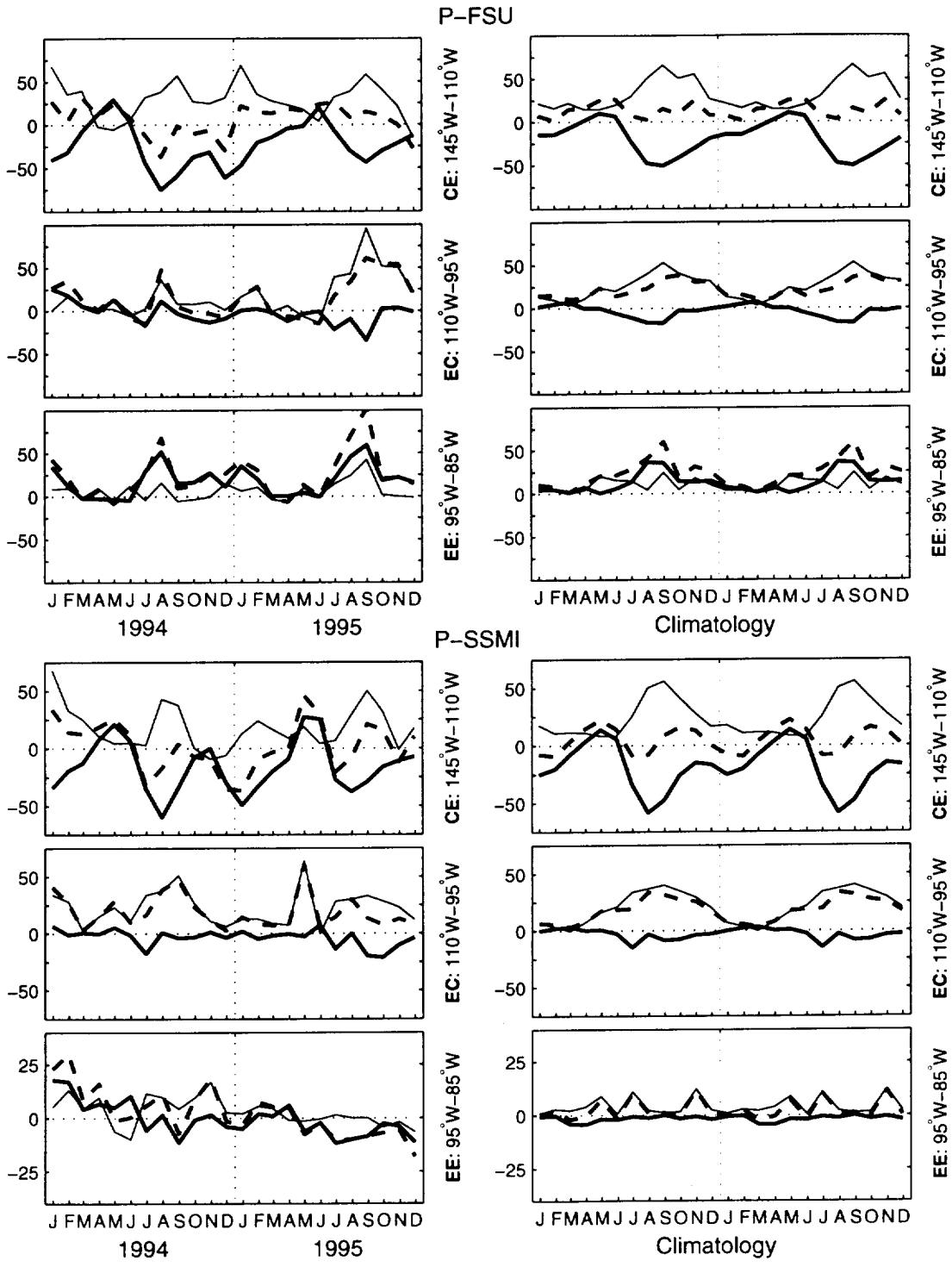

Figure 13: Low frequency (thick solid line) and eddy components (thin solid line) of the zonal advection term in the heat flux equation for the eastern Pacific. $Q_{zon.adv.} = -\rho_0 C_p u h \partial T/\partial x$ curves (dashed lines) are the same as in figures 12 and 11.